Published in final edited form as:
Nat Microbiol. ; 2: 17078. doi:10.1038/nmicrobiol.2017.78.

Multi-virion infectious units arise from free viral particles in an enveloped virus

José M. Cuevas[1,2], **María Durán-Moreno**[1], and **Rafael Sanjuán**[1,2,*]

[1]Institute for Integrative Systems Biology (I2SysBio), Universitat de València, Spain

[2]Department of Genetics, Universitat de València, València, Spain

Abstract

Many animal viruses are enveloped in a lipid bilayer uptaken from cellular membranes. Since viral surface proteins bind to these membranes to initiate infection, we hypothesized that free virions may also be capable of interacting with the envelopes of other virions extracellularly. Here, we demonstrate this hypothesis in the vesicular stomatitis virus (VSV), a prototypic negative-strand RNA virus composed by an internal ribonucleocapsid, a matrix protein, and an external envelope1. Using microscopy, dynamic light scattering, differential centrifugation, and flow cytometry, we show that free viral particles can spontaneously aggregate into multi-virion infectious units. We also show that, following the establishment of these contacts, different viral genetic variants are co-transmitted to the same target cell. Furthermore, virion-virion binding can determine key aspects of viral fitness such as antibody escape. In purified virions, this process is driven by protein-lipid interactions probably involving the VSV surface glycoprotein and phosphatidylserine. Whereas we found that multi-virion complexes occurred unfrequently in standard cell cultures, they were abundant in other fluids such as saliva, a natural VSV shedding route2. Our findings contrast with the commonly accepted perception of virions as passive propagules, and show the ability of enveloped viruses to establish collective infectious units, which could in turn facilitate the evolution of virus-virus interactions and of social-like traits3.

Following infection of baby hamster kidney (BHK-21) cells, we purified VSV virions by gradient ultracentrifugation and imaged the virion suspension by transmission electron microscopy. This showed typical, bullet-shaped virions of approximately 175 × 65 nm in size, but also revealed the presence of virion-virion contacts (Fig. 1a; Supplementary Fig. 1a-c). Ultrathin sections of agar-encased virions further suggested the involvement of envelope proteins in these contacts (Fig. 1b, Supplementary Fig. 1d). Such interactions were also observed by negative staining, which allowed visualization of the spikes of the surface glycoprotein (VSV-G) protruding from the envelope (Fig. 1c; Supplementary Fig. 1e-h).

Corresponding author. Correspondence and requests for materials should be addressed to R.S. rafael.sanjuan@uv.es. Address: Institute for Integrative Systems Biology (I2SysBio). C/Catedrático José Beltrán 2, 46980 Paterna, Valencia, Spain.

Author contributions. M.D-M. and J.M.C contributed equally to this work and performed all experiments. R.S. conceived the study, supervised the experiments, analyzed the data, and wrote the article.

Competing interests. The authors declare no competing interests.

Europe PMC Funders Author Manuscripts

We then used dynamic light scattering (DLS) to infer the hydrodynamic diameter (HD) of purified virions (Fig. 1d-g). Consistent with the VSV size, the HD harmonic mean (z-average) of viral particles was 170.7 ± 1.0 nm. However, we found significantly higher z-averages when virions were incubated at 37°C (pH 7.4) for various times (t-tests: $P < 0.001$), and this shift was accompanied by an increase in HD variance. After 1 h at 37°C, an estimated 91.8% of light scattering intensity was associated to particles with HD > 300 nm, as opposed to only 2.9% in non-incubated virions . Virion aggregation was further demonstrated by nanoparticle tracking analysis (NTA; Supplementary Videos 1 and 2). Longer incubation times (2 h, 4 h, overnight) yielded particle sizes falling outside the range of values than can be reliably measured by DLS and NTA (> 1 μm) and, after overnight incubation, virion aggregates were easily observed under a light microscope (Supplementary Fig. 2). In contrast to the extensive aggregation found at 37°C, incubation of virions at 25°C produced little or no change in particle size (Fig. 1d-g).

To test whether aggregates were infectious, purified virions were incubated at 37°C for various times and then used to infect BHK-21 monolayers to determine viral titers (plaque forming units, PFU per mL). The viral titer decreased more than two orders of magnitude after 2 h at 37°C (Fig. 1h). This could be attributed to virion degradation or aggregation. To test whether, as a result of aggregation, infectivity was increasingly associated to high-weight, multi-virion PFUs, we used low-speed centrifugation (10 min at 5000 g). After 2 h at 37°C the majority of PFUs (94.0 ± 1.4%) were located in the pellet, as opposed to only 7.3 ± 1.5% in controls kept at 4°C (Fig. 1i). High-weight PFUs were also detected using different incubation times and centrifugation speeds (Fig. 1j). Hence, VSV aggregation leads to an increased virion:PFU ratio.

To assess whether aggregated virions can be co-transmitted to the same target cells, we used two VSV recombinants encoding mCherry and GFP. Purified virions of each type were prepared separately and used to infect BHK-21 cells at low multiplicity of infection (MOI, defined as PFU/cell at inoculation), such that co-infection should be infrequent. Flow cytometry analysis at 6 h post inoculation (hpi) showed that, as expected, the fraction of red/green doubly fluorescent cells was low (0.13%-0.14% versus 0.15%-0.17% expected by chance). In contrast, when the VSV-GFP and VSV-mCherry stocks were co-incubated at 37°C for 2 h prior to inoculation, doubly fluorescent cells increased by 20-fold (2.98%-3.36%) and became nearly as abundant as red/green singly fluorescent cells (Fig. 2a). Using a probabilistic model (Supplementary Fig. 3), we inferred that 61.2% of all virions in the inoculum had bound to other virions and formed dual infectious units after 2 h at 37°C, whereas this fraction was 32.1% after 0.5 h at 37°C (Supplementary Table 1). Therefore, virion aggregation leads to the co-transmission of multiple viral genomes to the same cells. In contrast, a much weaker increase in co-infection rates was obtained when virions were pre-incubated at 25°C (0.29%-0.67% doubly-fluorescent cells; 2.7% dual infectious units by flow cytometry; Fig. 2a). The probabilistic analysis of virion-virion binding based on GFP/mCherry cell counts will be further used below, referred to as the co-fluorescence test.

We then set out to test whether virion-virion binding could promote functional interactions between different genetic variants of the virus. For this, we used an engineered VSV mutant

(A3853C) resistant to an anti-VSV-G neutralizing MAb4. As expected, the A3853C mutant grew normally in BHK-21 cells cultured with MAb, whereas viruses not carrying this mutation (WT) were unable to form plaques. In contrast, when a constant volume of the A3853C stock was pre-incubated (37°C, 2 h) with increasing amounts of the WT (5:1, 5:5, 5:10, and 5:20), the A3853C plaque forming efficiency in the presence of MAb decreased (1.2-fold, 7.7-fold, 11-fold, and 18-fold, respectively; t-tests: $P < 0.05$ for 5:1 and $P < 0.001$ for all other combinations; Fig. 2b). Hence, the WT had a dominant negative effect on the MAb-resistant mutant, suggesting that hybrid A3853C/WT virion aggregates were neutralized. Similar results were obtained when mixed virions were treated with MAb prior to cell inoculation instead of during plaque development, indicating that neutralization of hybrid virion complexes occurred before the first infection cycle (Fig. 2b).

To investigate possible molecular mechanisms involved in virion-virion binding, we first digested VSV-GFP with trypsin to remove VSV-G and other surface proteins from the envelope. This should abolish infectivity, since the VSV-G protein is required for cell attachment and entry. After purifying the digested virions, we infected BHK-21 cells at low MOI with an approximately 1:1 mixture of trypsin-digested VSV-GFP virions and intact VSV-mCherry virions. Flow cytometry at 6 hpi yielded 4.4% and 5.4% of mCherry-positive cells in two independent assays, but minimal GFP counts (0.030% and 0.022%, respectively) as well as extremely infrequent doubly fluorescent cells (0.015% and 0.019%, respectively; Fig. 3a; Supplementary Table 2), as expected. In contrast, when trypsin-digested VSV-GFP and intact VSV-mCherry virions were co-incubated at 37°C for 2 h prior to cell inoculation, doubly-fluorescent cells increased >300-fold (5.5% and 7.6% in two independent assays) and became similarly abundant as singly mCherry fluorescent cells (5.4% and 5.6%, respectively). This shows that the G protein of one virion is sufficient for promoting the entry of another, bound virion. It also shows that the surface proteins of VSV-GFP virions were not required for binding VSV-mCherry virions and, hence, that aggregation is not driven by protein-protein interactions. Unexpectedly, singly GFP-positive cells also increased following virion co-incubation (1.9% and 2.8%). Stronger and/or earlier GFP fluorescence compared to mCherry might have led us to erroneously assign some doubly fluorescent cells as GFP-only cells and, hence, to underestimate virion-virion binding and co-transmission. Alternatively, even if both virion types co-entered the same cells, early stochastic loss of one of the two variants could have occurred in some cases. Supporting this possibility, the increase in GFP-positive cells was less pronounced when flow cytometry was repeated at an earlier time point (4 hpi; Supplementary Table 2).

DLS indicated that virion aggregation was fully inhibited in the presence of trypsin (Fig. 3b), showing that the process is dependent on virion surface proteins. Together with the above results, this indicates that virion-virion binding is driven by protein-lipid interactions. The VSV envelope, which is uptaken from the plasma membrane of infected cells, is mainly composed of cholesterol, sphingomyelin, GM3 ganglioside, phosphatidylcholine, phosphatidylethanolamine, and phosphatidylserine (PS)5. Early work suggested that PS might be the VSV cellular receptor but this was later rejected because, in healthy cells, PS is located in the internal plasma membrane leaflet and hence is not available to virions6. However, VSV-G can bind PS through electrostatic interactions7,8. We found that aggregation was enhanced in the presence of phospholipase C (PLC), which hydrolyzes

several phospholipids but not PS9. We then performed DLS assays in the presence of PS-specific phospholipase A1α (PLA1A). As opposed to PLC, virion aggregation was diminished by PLA1A. Annexin V, a highly-specific PS-binding protein10, also inhibited aggregation partially. These data strongly suggest that interactions between VSV-G and PS are involved in virion-virion binding. The reason why PLC promoted aggregation is unclear. PLC might increase the surface exposure of PS, or envelope disruption produced by PLC treatment might expose matrix proteins, which could then interact with VSV-G.

In addition to VSV-G, the viral envelope also contains other, less abundant cellular proteins of unknown functional relevance for the virus. In virions egressed from BHK-21 cells, the second most abundant surface protein after VSV-G is Lrp111, a member of the LDL receptor family. Since LDL receptors are used for VSV cell attachment and entry12, we sought to test whether interactions between VSV-G and Lrp1 may also contribute to virion-virion binding. For this, we performed DLS assays in the presence of RAP, an Lrp1 inhibitor that prevents ligand binding13. We found a minimal effect of RAP on z-average values, thus providing no support for this hypothesis (Fig. 3b).

All the above experiments were conducted using high-titer, purified virions, raising the question whether virion-virion binding could take place under more physiological conditions. To test this in the context of an infected cell culture, we inoculated BHK-21 monolayers with VSV-mCherry at high MOI (10 PFU/cell), such that the vast majority of cells were infected by this inoculum. After 45 min absorption and 4 h incubation in infection medium (DMEM with 2% FBS), we added ca. 10^9 PFU of VSV-GFP to the cultures, and collected supernatants 3 h later for analysis. Superinfection exclusion should block entry of VSV-GFP14. Furthermore, internalized VSV-GFP virions could not have replicated and released progeny within 3 h. Consistently, flow cytometry indicated that < 0.1% of the cells were GFP-positive at the time of sampling. Hence, direct interaction between VSV-GFP and VSV-mCherry virions could only have taken place extracellularly. To assess whether the collected supernatants contained virion aggregates, we used the co-fluorescence test. According to our probabilistic model (Supplementary Fig. 3), 5.9 ± 1.0 % of virions had formed dual infectious units, as opposed to an estimated – 0.18 ± 0.62% in controls in which the two viruses were not co-incubated. Hence, multi-virion infectious units arose in these cell cultures, albeit to a much lower extent than in gradient-purified virions.

The limited amount of virion aggregation found above could be attributed to the lower viral titer used (10^9 versus 10^{11} PFU/mL for purified virions) or to the physicochemical properties of the media employed. To explore this, we co-incubated 10^9 PFU/mL of each VSV-mCherry and GFP-VSV in different media (Fig. 4a; Supplementary Table 1). Whereas virion-virion binding at 37°C was unfrequent in DMEM with 2% FBS (3.6 ± 1.0% virions in dual infectious units after overnight incubation) or FBS alone (1.2 ± 0.4% after 2 h), it was more abundant in human plasma (6.4% to 17.6% after 2 h depending on the subject). Since the oral cavity is a major site of infection for VSV, causing stomatitis, we set out to test for virion aggregation in saliva. We first collected samples from four volunteers. For a starting titer of ca. 10^9 PFU/mL of each VSV-GFP and VSV-mCherry, the co-fluorescence test indicated that the fraction of virions forming dual infectious units ranged from 31.2% to 35.0% in three individuals and was extremely high for the fourth individual (94.9%) after 1

h co-incubation at 37°C (longer incubation times could not be assayed due to loss of infectivity). When the experiment was repeated using saliva from the fourth donor but with a starting titer of only 10^7 PFU/mL, virions in dual infectious units were still highly abundant (50.8%), confirming that virion-virion binding depended more on the properties of the medium than on virion concentration. To ascertain whether these results could be reproduced in saliva from a more typical VSV host, we used four cows. Rapid loss of infectivity was again observed in saliva from 3/4 cows. After only 15 min at 37°C the fraction of virions in dual infectious units ranged from 46.9% to 88.5% in three of the samples, whereas saliva from the fourth cow showed little or no viral titer loss and a lower level of aggregation (9.3%). We conclude that VSV aggregation and co-transmission of variants is promoted by human and cow saliva. Overall, we found a significant correlation between the rate of titer loss and levels of aggregation across media (DMEM, plasma, human saliva, and bovine saliva), consistent with our above finding that aggregation increases the virion:PFU ratio (Fig. 4b).

Early electron microscopy studies indicated that viral particles can form aggregates in a variety of viruses including tobacco mosaic virus15, poxviruses16, influenza virus17, VSV18, and poliovirus19, but this was mainly viewed from a technical standpoint and the molecular basis and implications have remained largely unexplored. More recent work in which we analyzed the VSV genetic diversity produced by single infected cells suggested that infectious units could be constituted by multiple virions20. Furthermore, aggregation has been recently found to favor the co-transmission of different genetic variants in poliovirus and to increase plaque formation efficiency in highly mutated populations, suggesting genetic complementation21. Here, we have investigated the mechanism and implications of aggregation in VSV, a prototypic enveloped, negative strand RNA virus (see Supplementary Fig. 4 for a graphical abstract of our findings). We have also found that virion-virion binding occurs strongly in saliva, moderately in plasma and unfrequently in standard culture media. This suggests that the process could be relevant *in vivo*, but also that typical virus culturing conditions may not be suited for studying it. VSV produces ulcers and vesicles in the oral and nasal mucosa, which can contain 10^9 PFU/mL of VSV22. The saliva is an important route of viral shedding and could act as a vehicle for transmission to plant-eating arthropod vectors2,23. We found that the VSV titer decayed rapidly in virion-aggregating saliva, from 10^9 PFU/mL to $< 10^7$ PFU/mL after 15 min in some cases (Fig. 4b). Experimentally inoculated farm animals reach maximal viral loads that vary broadly, but typical maximal values are on the order of 10^6-10^8 TCID50/mL in the oral cavity, nose swabs, and other body compartments24–26. We suggest that, in addition to dilution and degradation, the lower titers observed in some body fluids compared to intra-lesion titers may be in part influenced by virion aggregation. As such, virion aggregation could be viewed as an antiviral mechanism conceptually akin to antibody-mediated agglutination. However, it is also possible that aggregates of virions may have some advantage in terms of faster initiation of infection, increased survival in the environment, or other fitness benefits. Future work may shed light on these questions.

Our results indicate that, although virion-virion binding can take place within a realistic range of virion concentrations, it depends critically on the composition of the medium. These physicochemical determinants remain to be elucidated. Candidate factors are viscosity

and ionic strength. Saliva, plasma, serum, and the buffer used for virion purification all have viscosity values ≥ 1 mPa s, compared to 0.69 mPa s for water at 37°C. We should note that virion aggregation and fusion of viral envelopes has been previously observed under acidic conditions (pH < 6.5), in a process that mimics fusion with endosomal membranes after cell entry27. In contrast, the extracellular virion-virion binding process described here occurs at neutral pH. We identified VSV-G and PS as the most likely molecular actors of virion-virion binding in purified virions, but it remains to be explored whether the same molecular interactors drive aggregation in plasma and saliva. Saliva may contain additional proteins or other macromolecules that drive this process.

PS is an endocytosis signal that triggers physiological mechanisms for recycling cellular debris28. By incorporating PS into their envelopes, many viruses exploit these pathways to entry into cells, a strategy known as apoptotic mimicry29. Also, recent work has shown that, in enteroviruses, encapsulation into PS vesicles enables the simultaneous extracellular transmission of multiple virions30. This suggests that PS may play a role in the transmission of various types of viruses, through different mechanisms.

Under the notion that virions function as independent infectious units, the evolution virus-virus interactions, including cooperation and conflict, is difficult to envisage because, although co-infection of cells with multiple virus variants is possible under high-MOI regimes, the inherent population bottlenecks associated with inter-cellular, organ-to-organ, and host-to-host transmission31 would make such interactions necessarily short-lived. In contrast, multi-virion complexes and other forms of collective infectious units may enable the co-transmission of different genetic variants of a virus regardless of population bottlenecks3. Our findings could hence contribute to explaining why some defective mutants, which are unable to replicate in the absence of a functional variant, can nevertheless undergo sustained among-host transmission, as has been found in dengue32 and influenza33 viruses. In turn, this could have implications for the use of transmissible interfering viruses as an anti-viral intervention strategy34,35.

Finally, our results contrast with the generally accepted view of virions as individual, passive carriers of viral genetic information. Given that PS is a ubiquitous component of membranes and that early electron microscopy studies reported virion aggregation in several enveloped viruses, similar virion-virion binding and co-transmission processes might take place in other viruses. Future work may elucidate how virion aggregates and other types of multi-virion infectious units determine social-like virus-virus interactions.

Methods

Cells, viruses, and reagents

BHK-21 fibroblasts were obtained from the American Type Culture Collection (ATCC) and were not authenticated further. BHK-21 cells are not listed in the ICLAC database of commonly misidentified cell lines. Cells were cultured in Dulbeco's modified Eagle's Medium (DMEM) supplemented with 10% foetal bovine serum (FBS) at 37°C in a 5% CO_2 humidified incubator, and tested mycoplasma negative by PCR. The following commercially available reagents were used: trypsin (0.125%; GIBCO, 15090-046), *Clostridium welchii*

PLC (10 mg/mL; Sigma-Aldrich, P7633), human PLA1A (1 mg/mL; ProSpec, ENZ-794), human placental annexin V (7.5 mg/mL; Sigma-Aldrich, A9460), and mouse RAP (0.25 mg/mL; Sino Biological Inc., 50281-M08H-50). A neutralizing MAb against VSV-G was obtained in house from a mouse hybridoma cell line, as described previously36. An infectious Indiana VSV cDNA clone37 was used for introducing the A3853C mutation by site-directed mutagenesis, as described previously4. The A3853C mutation is selectively neutral in the absence of neutralizing MAb4. Reverse genetics was also used to clone the mCherry and GFP genes at the intergenic region between the G and L genes. VSV-mCherry and VSV-GFP virions were used for microscopy, DLS, and centrifugation assays. The morphology and physical properties of these virions should be identical to those of the wild type, since GFP and mCherry are not structural proteins. In antibody neutralization assays VSV-GFP was also used as a surrogate wild type.

Saliva and plasma collection

Saliva was collected from cows (*Bos taurus* females, strain Frisona) at a local farm (La Muntanyeta Coop. V.) under veterinary supervision, following standard non-invasive procedures that guaranteed animal welfare, in compliance with Spanish legislation. Animals were between two and six years old and were selected randomly by the veterinary. We found no correlation between age and aggregation status. Human saliva was provided by four volunteers, who all gave informed consent. This included three men and one woman aged between 25 and 41 years old, with no observed correlation between aggregation status and age. The strongest aggregating saliva was from the woman, which may be coincidental. The sample size (four individuals for cows and humans) was selected for convenience, with no a priori statistical consideration. Both types of saliva were filtered with a 0.45 μm cellulose filter, aliquoted, and stored at –70°C until use. Plasmas were obtained from blood donors at the Hospital General de Valencia (Spain) by collecting the higher fraction of centrifuged blood samples (1200 g, 10 min, 4°C) and stored at –70°C until use. The procedure for collecting plasma was approved by the Ethical Committee of the Universitat de València.

Plaque assays

Confluent BHK-21 monolayers were used for virus titrations. The monolayers were inoculated for 45 min under standard culturing conditions (37°C, 5% CO_2) and then overlaid with DMEM supplemented with 2% FBS and 0.5% agarose. After 20 h, cells were fixed with 10% formaldehyde, stained with 2% crystal violet in 10% formaldehyde, and plaques were counted.

Virion purification

Stocks of VSV-mCherry, VSV-GFP, and VSV-A3853C were prepared by inoculating eight BHK-21 confluent T175 flasks at an MOI of 0.01 PFU/mL and collecting supernatants upon appearance of the first obvious cytopathic effects (ca. 20 hpi). Large cellular debris were removed by spinning (780 g, 5 min) and filtering (0.22 μm) supernatants. Virions were then pelleted at 30,000 g, 4°C, 1.5 h in a Beckman Coulter Avanti J25I centrifuge with a JA-14 rotor. The pellet was resuspended in 2 mL NaCl 0.6%, Tris 0.6%, EDTA.Na_2.$2H_2O$ 0.02% buffer (pH 7.4), laid on a 5-50% iodixanol (Optiprep, Sigma) gradient in ultra-clear thin-walled tubes, and ultra-centrifuged at 160,000 g, 4°C, 1.5 h in a Beckman Optima L90 K

centrifuge with a SW41-Ti rotor. Approximately 700 μL of a whitish band generated at mid-gradient were collected, aliquoted, and stored immediately at –70°C. Final titers were on the order of 10^{11} PFU/mL for all viral stocks, as determined by plaque assays in BHK-21 cells.

Microscopy

Purified virions were fixed in 4% paraformaldehyde 5% glutaraldehyde solution in phosphate buffer 0.1 M by incubating the mix at room temperature for at least 1 h. For direct observation of the virion suspension, 5 μL of this mix were deposited onto formvar mesh grids and dried gently at room temperature. Grids were washed three times through contact with the surface of distilled water drop and immersed 5 min in 2% uranyl acetate drop for positive staining, or 1 min in 1.5% phosphotungstic acid for negative staining. After drying, grids were imaged and photographed under a Jeol JEM-1010 electron microscope. For observation of virions in cross section, the fixed preparations were encased in a 1% agar cone. The fixator was then removed by successive phosphate buffer 0.1 M washes, and preparations were post-fixed and stained with 2% osmium solution, dehydrated in a graded series of ethanol and stained during dehydration with 2% uranyl acetate in ethanol 70%. Samples were embedded in Durcupan epoxy resin and polymerized for 72 h at 70°C. Semi-thin sections (1.5 μm) were obtained using a Leica EM UC-6 ultra-microtome (Leica) and stained with 1% toluidine blue at 70°C for optical microscopy. Ultrathin sections (0.08 μm) were obtained with a diamond-tipped knife, stained with Reynold's lead citrate, and imaged by electron microscopy.

DLS

Since Brownian motion is determined by particle size, the temporal auto-correlation of light scattering decays at a rate that depends inversely on particle size, allowing inference of particle size (HD). For each assay, purified virions (10 μL) were fixed immediately (untreated control) or incubated at 37°C or 25°C as indicated prior to fixation, kept >1 h at room temperature, diluted 1:10 in ultrapure water, placed in a disposable polystyrene low-volume cuvette for DLS, and analyzed in a Malvern Zetasizer NanoZS device. Water viscosity was assumed for particle sizing, and all measurements were taken at 25°C. Control assays were performed to ensure that fixation/dilution did not modify the particle size distribution compared to non-fixed virions. In aggregation inhibition assays, all tested inhibitors (trypsin, PLC, PLA1A, annexin V, or RAP) were previously diluted 1/5 in a buffer mimicking the composition of the buffer of the VSV purified virions (iodixanol 24%, NaCl 0.3%, Tris 0.7%, EDTA.Na_2.$2H_2$0 0.02%, pH 7.4) to ensure that the observed changes in aggregation were not due to differences in the buffers used, and 1 μL of this dilution was added to a purified virion aliquot (10 μL) immediately before incubation at 37°C. In these assays, additional controls were included in which the reagents were added post-fixation to ensure that no changes in DLS measurements were observed. Data were analyzed by the cumulants method, which allows inference of the average particle HD from the first-order auto-correlation decay rate, and of particle HD variance from the second-order decay rate38. Following manufacturer's recommendations, mean HD was quantified using the z-average, defined as the harmonic intensity averaged HD (also known as cumulants mean), and HD variance was quantified using the polydispersity index. The distribution of light scattering

Europe PMC Funders Author Manuscripts

intensity as a function of particle size, as provided by the Zetasizer software, was exported to a plain text file and graphed.

Nanoparticle tracking analysis

This technique is based on video tracking the light diffraction of individual nanoparticles to characterize their Brownian motion and infer their size. Purified virions were loaded into a NanoSight NS300 equipment (Malvern) with the aid of a syringe pump to increase particle flow through the chamber, and analyzed by built-in software using default parameters.

Centrifugation assays

Purified virions were incubated at 37°C or 4°C (untreated controls) in separate 8 μL aliquots, mixed with 92 μL DMEM 1X, and centrifuged once at the indicated speeds. The supernatant (S) was collected for titration, and the pellet was washed once with 1 mL DMEM 1X using the same centrifugation speed and time, and then resuspended in 100 μL DMEM 1X (P), after discarding the supernatant. The S and P fractions were titrated by the plaque assay, and the fraction of PFUs in the pellet was calculated as the P/S titer ratio.

Flow cytometry and co-fluorescence test

VSV-mCherry and VSV-GFP virions were co-incubated as indicated, serially diluted in DMEM 1X, and used to inoculate a monolayer of approximately 3×10^6 confluent BHK-21 cells. For untreated controls, VSV-mCherry and VSV-GFP were serially diluted separately and then used to infect BHK-21 cells, such that co-infection should only take place if two virions entered independently in the same cell. After 45 min incubation of the inoculum (37°C and 5% CO_2), cultures were overlaid with DMEM 1X supplemented with 2% FBS and incubated for 7 h. Based on the growth dynamics of VSV in BHK-21 cells, this should allow for only one cell infection cycle. However, since growth is not perfectly synchronous, initiation of a second cycle probably occurred in some cases. Additionally, GFP and mCherry proteins may diffuse to other cells. In any case, these potential problems would lead to underestimating aggregation, because a fraction of these second-cycle cells might receive only one of the variants despite the initial cell being co-infected by the two variants. Cells were then detached using trypsin-EDTA, resuspended in DMEM 1X containing 10% FBS, washed with PBS 1X by centrifugation (1500 rpm, 5 min), resuspended in 1 mL 4% paraformaldehyde for fixation, and incubated overnight at 4°C. The fixator was removed and washed with PBS 1X by centrifugation (700 rpm, 10 min, twice), cells were resuspended in PBS 1X at a density of ca. 10^6 cells/mL, and 10^5 events per sample were analyzed in a Becton Dickinson LSRFortessa flow cytometer equipped with 488 nm and 561 nm lasers for GFP and mCherry excitation, respectively. Controls of non-infected cultures as well as of cultures singly infected with VSV-mCherry or VSV-GFP were run in parallel and used to delineate quadrants manually. Cell counts were used to infer the fraction of virions bound to other virions in the inoculum, as detailed in Supplementary Fig. 3.

MAb neutralization assays

Aliquots of purified VSV-A3853C virions (5 μL) were mixed with different volumes of VSV-GFP as indicated, maintained at 37°C for 2 h, serially diluted, and used for plaque

assays in which the infected cells were cultured with 10% (v:v) of a MAb -containing stock obtained directly from a mouse hybridoma supernatant. A control plaque assay without MAb was run in parallel. In additional experiments, virion mixes were incubated at 37°C for 2 h, treated with one volume of the MAb suspension (25°C, 30 min), and used for plaque assays in the absence of the MAb. Cultures were fixed and stained as indicated above (plaque assays).

Statistical notes

Names of statistical tests and the number of replicate assays are shown in the text or figure legends. All tests were two-sided. The numbers of replicate assays were not chosen to ensure a particular statistical power or detect pre-specified effect sizes. No samples were excluded from the analysis. No randomization methods were required to allocate or process experimental groups, and no blinding was used. Wherein indicated, log transformation of data was used. This is recommended for use of parametrical tests when data span several orders of magnitude and have asymmetrical definition intervals (e.g. viral titers). The SEM was used to estimate variation within each data group, or raw data points are shown alternatively. Normality tests were not implemented because they show low statistical power for small datasets as those used here and are thus non-informative (t-tests are robust to deviations from normality). As a conservative approach, unequal variances were assumed in all tests.

Data availability

Relevant data are with the manuscript and associated supplementary information. No new protein, DNA, or RNA sequence data, macromolecular structures, crystallographic data or microarray data requiring deposition in public repository were produced.

Supplementary Material

Refer to Web version on PubMed Central for supplementary material.

Acknowledgments

We thank Drs. David Vie, Ana Flores, Raquel Garijo, and Silvia Torres for technical assistance, and personnel from La Muntanyeta Coop. V. for providing us access to cows. This work was financially supported by grants from the European Research Council (ERC-2011-StG- 281191-VIRMUT and ERC-2016-CoG-724519-Vis-à-Vis) and the Spanish MINECO (BFU2013-41329) to R.S., and by a Ramón y Cajal contract to J.M.C.

References

1. Ge P, et al. Cryo-EM model of the bullet-shaped vesicular stomatitis virus. Science. 2010; 327:689–693. [PubMed: 20133572]
2. Letchworth GJ, Rodríguez LL, Del Cbarrera J. Vesicular stomatitis. Vet J. 1999; 157:239–260. [PubMed: 10328837]
3. Sanjuán R. Collective infectious units in viruses. Trends Microbiol. 2017; 25:402–412. DOI: 10.1016/j.tim.2017.02.003 [PubMed: 28262512]
4. Sanjuán R, Moya A, Elena SF. The distribution of fitness effects caused by single-nucleotide substitutions in an RNA virus. Proc Natl Acad Sci USA. 2004; 101:8396–8401. [PubMed: 15159545]

5. Kalvodova L, et al. The lipidomes of vesicular stomatitis virus, semliki forest virus, and the host plasma membrane analyzed by quantitative shotgun mass spectrometry. J Virol. 2009; 83:7996–8003. [PubMed: 19474104]
6. Coil DA, Miller AD. Phosphatidylserine is not the cell surface receptor for vesicular stomatitis virus. J Virol. 2004; 78:10920–10926. [PubMed: 15452212]
7. Carneiro FA, et al. Probing the interaction between vesicular stomatitis virus and phosphatidylserine. Eur Biophys J. 2006; 35:145–154. [PubMed: 16184389]
8. Hall MP, Burson KK, Huestis WH. Interactions of a vesicular stomatitis virus G protein fragment with phosphatidylserine: NMR and fluorescence studies. Biochim Biophys Acta. 1998; 1415:101–113. [PubMed: 9858700]
9. Mac Farlane MG. The biochemistry of bacterial toxins; the enzymic specificity of Clostridium welchii lecithinase. Biochem J. 1948; 42:587–590.
10. Tait JF, Gibson D. Phospholipid binding of annexin V: effects of calcium and membrane phosphatidylserine content. Arch Biochem Biophys. 1992; 298:187–191. [PubMed: 1388011]
11. Moerdyk-Schauwecker M, Hwang SI, Grdzelishvili VZ. Cellular proteins associated with the interior and exterior of vesicular stomatitis virus virions. PLoS One. 2014; 9:e104688. [PubMed: 25105980]
12. Finkelshtein D, Werman A, Novick D, Barak S, Rubinstein M. LDL receptor and its family members serve as the cellular receptors for vesicular stomatitis virus. Proc Natl Acad Sci USA. 2013; 110:7306–7311. [PubMed: 23589850]
13. Prasad JM, Migliorini M, Galisteo R, Strickland DK. Generation of a potent low density lipoprotein receptor-related protein 1 (LRP1) antagonist by engineering a stable form of the receptor-associated protein (RAP) D3 domain. J Biol Chem. 2015; 290:17262–17268. [PubMed: 26013822]
14. Simon KO, Cardamone JJ Jr, Whitaker-Dowling PA, Youngner JS, Widnell CC. Cellular mechanisms in the superinfection exclusion of vesicular stomatitis virus. Virology. 1990; 177:375–379. [PubMed: 2162110]
15. Bald JG, Briggs GE. Aggregation of virus particles. Nature. 1937; 140:111.
16. Galasso GJ, Sharp DG. Virus particle aggregation and the plaque-forming unit. J Immunol. 1962; 88:339–347. [PubMed: 13896316]
17. Wallis C, Melnick JL. Virus aggregation as the cause of the non-neutralizable persistent fraction. J Virol. 1967; 1:478–488. [PubMed: 4318956]
18. Galasso GJ. Quantitative studies on the quality, effects of aggregation and thermal inactivation of vesicular stomatitis virus. Arch Gesamte Virusforsch. 1967; 21:437–446. [PubMed: 4300742]
19. Floyd R. Viral aggregation: mixed suspensions of poliovirus and reovirus. Appl Environ Microbiol. 1979; 38:980–986. [PubMed: 44447]
20. Combe M, Garijo R, Geller R, Cuevas JM, Sanjuán R. Single-cell analysis of RNA virus infection identifies multiple genetically diverse viral genomes within single infectious units. Cell Host Microbe. 2015; 18:424–432. [PubMed: 26468746]
21. Aguilera ER, Erickson AK, Jesudhasan PR, Robinson CM, Pfeiffer JK. Plaques formed by mutagenized viral populations have elevated coinfection frequencies. MBio. 2017; 8:e02020–16. [PubMed: 28292984]
22. Marcus PI, Rodríguez LL, Sekellick MJ. Interferon induction as a quasispecies marker of vesicular stomatitis virus populations. J Virol. 1998; 72:542–549. [PubMed: 9420257]
23. Nunamaker RA, et al. Grasshoppers (*Orthoptera*: *Acrididae*) could serve as reservoirs and vectors of vesicular stomatitis virus. J Med Entomol. 2003; 40:957–963. [PubMed: 14765676]
24. Scherer CF, et al. Vesicular stomatitis New Jersey virus (VSNJV) infects keratinocytes and is restricted to lesion sites and local lymph nodes in the bovine, a natural host. Vet Res. 2007; 38:375–390. [PubMed: 17506968]
25. Smith PF, et al. Mechanical transmission of vesicular stomatitis New Jersey virus by *Simulium vittatum* (*Diptera*: *Simuliidae*) to domestic swine (*Sus scrofa*). J Med Entomol. 2009; 46:1537–1540. [PubMed: 19960709]

26. Smith PF, et al. Host predilection and transmissibility of vesicular stomatitis New Jersey virus strains in domestic cattle (*Bos taurus*) and swine (*Sus scrofa*). BMC Vet Res. 2012; 8:183–188. [PubMed: 23034141]
27. Libersou S, et al. Distinct structural rearrangements of the VSV glycoprotein drive membrane fusion. J Cell Biol. 2010; 191:199–210. [PubMed: 20921141]
28. Nagata S, Hanayama R, Kawane K. Autoimmunity and the clearance of dead cells. Cell. 2010; 140:619–630. [PubMed: 20211132]
29. Amara A, Mercer J. Viral apoptotic mimicry. Nat Rev Microbiol. 2015; 13:461–469. [PubMed: 26052667]
30. Chen YH, et al. Phosphatidylserine vesicles enable efficient en bloc transmission of enteroviruses. Cell. 2015; 160:619–630. [PubMed: 25679758]
31. Gutiérrez S, Michalakis Y, Blanc S. Virus population bottlenecks during within-host progression and host-to-host transmission. Curr Opin Virol. 2012; 2:546–555. [PubMed: 22921636]
32. Aaskov J, Buzacott K, Thu HM, Lowry K, Holmes EC. Long-term transmission of defective RNA viruses in humans and *Aedes* mosquitoes. Science. 2006; 311:236–238. [PubMed: 16410525]
33. Stack JC, Murcia PR, Grenfell BT, Wood JL, Holmes EC. Inferring the inter-host transmission of influenza A virus using patterns of intra-host genetic variation. Proc Biol Sci. 2013; 280 20122173.
34. Marriott AC, Dimmock NJ. Defective interfering viruses and their potential as antiviral agents. Rev Med Virol. 2010; 20:51–62. [PubMed: 20041441]
35. Notton T, Sardanyes J, Weinberger AD, Weinberger LS. The case for transmissible antivirals to control population-wide infectious disease. Trends Biotechnol. 2014; 32:400–405. [PubMed: 25017994]
36. Vandepol SB, Lefrancois L, Holland JJ. Sequences of the major antibody binding epitopes of the Indiana serotype of vesicular stomatitis virus. Virology. 1986; 148:312–325. [PubMed: 2417417]
37. Whelan SP, Ball LA, Barr JN, Wertz GT. Efficient recovery of infectious vesicular stomatitis virus entirely from cDNA clones. Proc Natl Acad Sci USA. 1995; 92:8388–8392. [PubMed: 7667300]
38. Hassan PA, Rana S, Verma G. Making sense of Brownian motion: colloid characterization by dynamic light scattering. Langmuir. 2015; 31:3–12. [PubMed: 25050712]

Europe PMC Funders Author Manuscripts

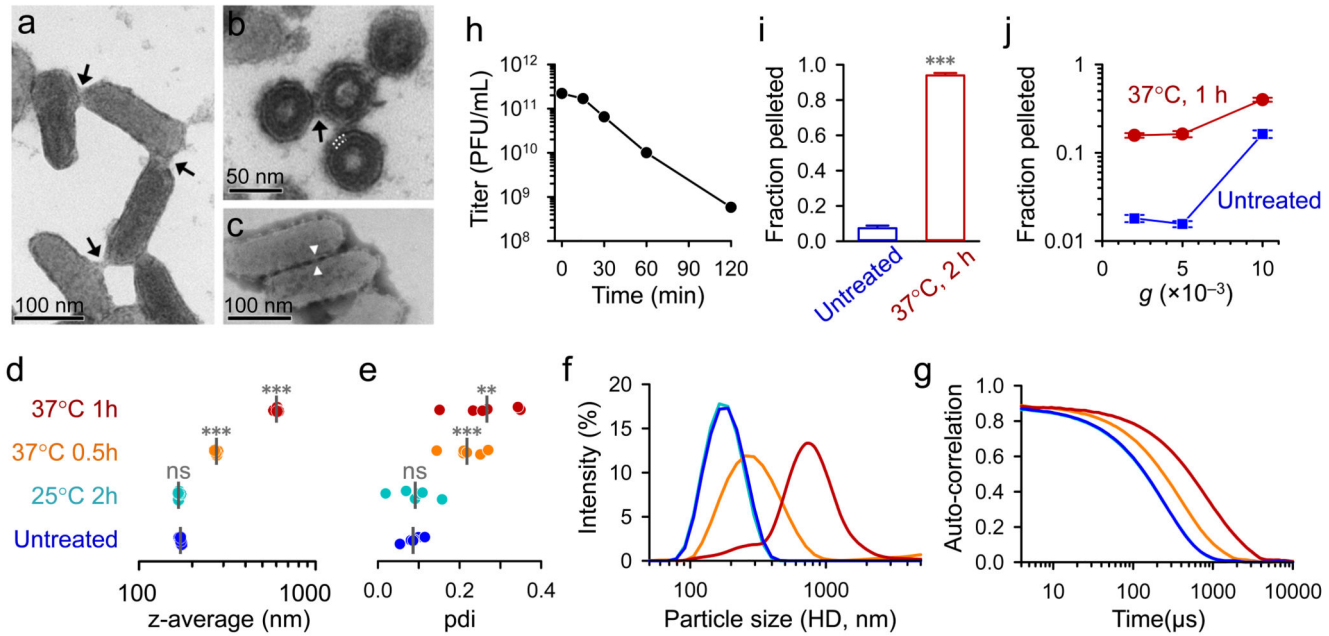

Fig. 1. Spontaneous aggregation of purified VSV virions.

Transmission electron micrographs of purified VSV virions (**a-c**), showing a virion suspension positively stained with uranyl acetate (**a**; arrows indicate contacts between virions), an ultrathin section of agar-encased virions (**b**; four virions are shown in trans section; the envelope bilayer is indicated with white dotted lines; the structure protruding from the envelope lipid bilayer, indicated with an arrow, probably corresponds to the envelope protein G), and a virion suspension negatively stained with phosphotungstic acid (**c**; the envelope protein is visible and appears to mediate virion-virion contacts, one of which is indicated). Additional micrographs are shown in Supplementary Fig. 1. Virions were subjected to DLS (**d-g**) by fixing virions immediately (untreated) or after incubation, as indicated. The z-average values obtained from six measurements are shown (**d**). Vertical grey lines indicate the mean z-average. Treatment effects were evaluated relative to the untreated group using t-tests (ns: $P > 0.05$; **: $P < 0.01$; ***: $P < 0.001$). **e.** Polydispersity indexes (pdi) obtained in the same set of measurements. Particle size distribution curves, expressed as the percentage total light scattering intensity (**f**) and raw auto-correlation data (**g**) are shown, where each curve is an average from the six measurements. **h.** Effect of aggregation on infectivity, as determined in BHK-21 cells by the plaque assay after incubating purified virions at 37°C for the indicated times. To assess PFU weight, virions were centrifuged directly (blue) or after 2 h incubation at 37°C (red), and the pellet and supernatant were titrated by the plaque assay (**i**; the pellet/supernatant titer ratio is represented). Pellet/supernatant titer ratios for increasing centrifugation forces (5 min spin) after incubating virions 1 h at 37°C are also shown (**j**). Error bars indicate the standard error of the mean from three assays.

Europe PMC Funders Author Manuscripts

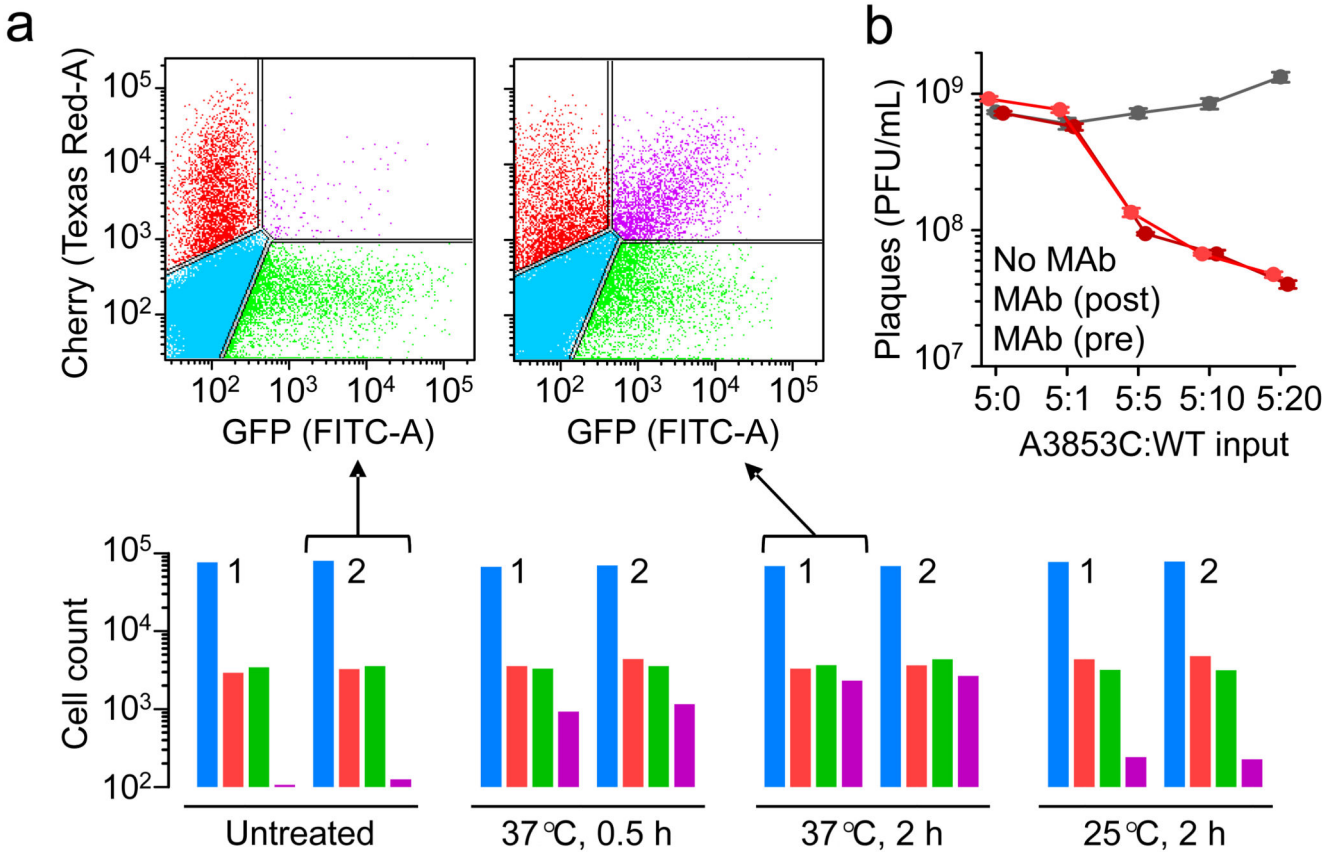

Fig. 2. Functional implications of multi-virion infectious units.

Proof of concept for the co-transmission of genetic variants was obtained by flow cytometry using two fluorescently labelled viruses (**a**). Cells were inoculated with VSV-mCherry and VSV-GFP, incubated 7 h, and counted (10^5 events per assay). Bottom: uninfected (blue), mCherry-positive (red), GFP-positive (green), and doubly fluorescent (purple) cell counts following direct inoculation with VSV-GFP and VSV-mCherry (untreated) or after co-incubation of the two virion types (0.5 h at 37°C, 2 h at 37°C, or 2 h at 25°C). Two independent assays (1, 2) are shown for each condition. Top: flow cytometry scatter plot from two of the experiments. The estimated fraction of total virions forming dual infectious units was inferred using a probabilistic model detailed in Supplementary Fig. 3. Data are provided in Supplementary Table 1. **b.** Effects of virion-virion binding on antibody escape. Plaque assays of the MAb-resistant (A3853C) and MAb-sensitive (WT) variants following pre-incubation of the two types of virions (37°C, 2 h) at different proportions (v:v): 5:0, 5:1, 5:5, 5:10, and 5:20. For each treatment, plaque assays were done in the absence of MAb (grey), adding MAb to the culture medium to inhibit plaque development (dark red) or adding MAb prior to cell inoculation to inhibit cell entry (light red). Data points indicate average titers (PFU/mL) obtained from three independent assays, and error bars indicate the standard error of the mean.

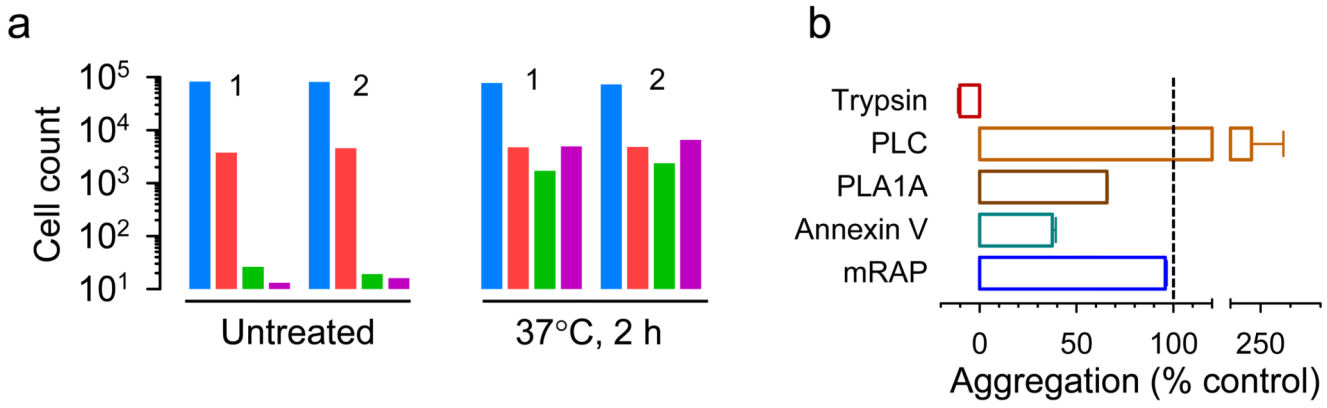

Fig. 3. Envelope protein-lipid interactions mediate virion-virion binding in VSV.

a. Co-fluorescence test. Cells were inoculated with VSV-mCherry and with pre-trypsinized VSV-GFP, and subsequently analyzed by flow cytometry (10^5 events per assay). Counts of uninfected (blue), mCherry-positive (red), GFP-positive (green), and doubly fluorescent (purple) cells after direct inoculation with the viral mix (untreated) or after co-incubation of the two virion types (37°C, 2 h) are shown. Two independent assays (1, 2) are shown for each condition. **b.** DLS assays showing the effects of various treatments on virion aggregation. Purified virions were incubated at 37°C for 1 h alone (control) or in the presence of trypsin, PLC, PLA1A, annexin V, or mouse RAP. The change in z-average relative to the average change in z-average obtained for controls is shown, i.e. Δ(z-average treatment)/Δ(z-average control). All assays were performed in triplicate and the error bar represents the standard error of the mean.

Europe PMC Funders Author Manuscripts

Europe PMC Funders Author Manuscripts

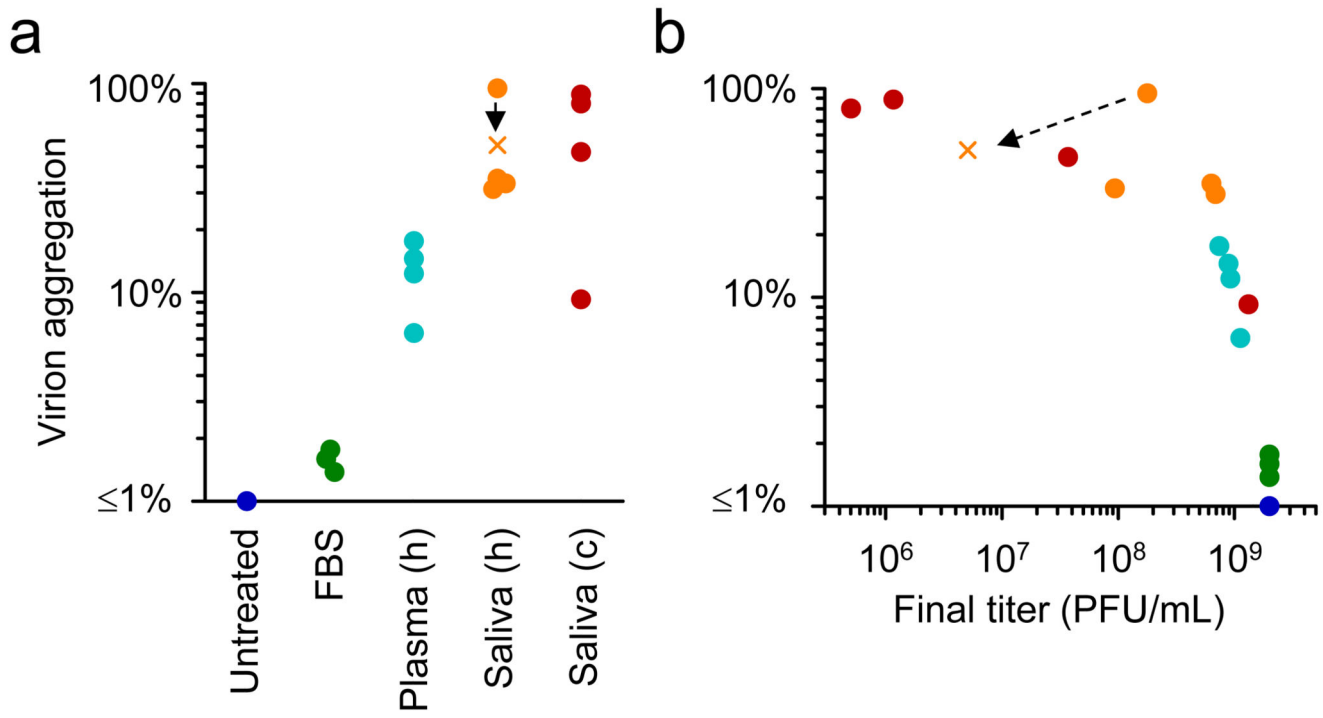

Fig. 4. VSV virion-virion binding in cell culture media, plasma, and saliva.

a. In each of the fluids tested, ca. 10^9 PFU/mL of each VSV-GFP and VSV-mCherry were co-incubated at 37°C for 2 h in FBS or human (h) plasma, 1 h in human saliva, or 15 min in cow (c) saliva, or not co-incubated (untreated). For one of the human salivas, the test was done both at 10^9 PFU/mL (circle) and 10^7 PFU/mL (cross). The amount of virion aggregation is represented as the fraction of virions forming dual PFUs estimated by the co-fluorescence test (see Methods and Supplementary Fig. 3; cell counts are available from Supplementary Table 1). For plasma and saliva, each data point corresponds to an individual donor (human/cow) and represents the average of two independent assays. For FBS, three independent assays are plotted. For untreated viruses, the estimated amount of virion aggregation fluctuated around zero (from –1.4% to 1.9% in six independent assays) and is shown as a single blue dot at the lower-limit of the plot range. **b.** Virion aggregation as a function of the final titer (i.e. after incubation), showing the correlation between titer loss and aggregation.